

1 **Full Title: Acetylcholine regulates pulmonary inflammation and facilitates the transition from active**
2 **immunity to tissue repair during respiratory viral infection**

3
4 **Short title:** Acetylcholine and influenza infection

5
6 Alexander P. Horkowitz^{1,2#a}, Ashley V. Schwartz³, Carlos A. Alvarez^{1,2#b}, Edgar B. Herrera¹, Marilyn L.
7 Thoman¹, Dale A. Chatfield⁴, Kent G. Osborn⁵, Ralph Feuer², Uduak Z. George³, Joy A. Phillips^{1*}

8
9 1 Donald P. Shiley Biosciences Center, San Diego State University, San Diego, California, USA

10 2 Department of Biology, San Diego State University, San Diego, California

11 3 Department of Mathematics and Statistics, San Diego State University, San Diego, California, USA

12 4 Department of Chemistry, San Diego State University, San Diego, California, USA

13 5 Office of Animal Research, University of California, San Diego, San Diego, California, USA

14 #a Current Address: Sanford Burnham Prebys Medical Discovery Institute, San Diego, California, USA

15 #b Current Address: Department of Pathology, Case Western Reserve University School of Medicine,
16 Cleveland, Ohio, SA

17
18 *Corresponding Author:

19 *E-mail: jphillips@sdsu.edu (JP)

20
21 **Author Contributions**

22 Conceived and designed the experiments: AH MT DC RF JP.

23 Performed the experiments: AH CA EH MT DC RF JP.

24 Analyzed the data: AH AS CA EH MT DC KO RF UG JP

25 Contributed reagents/materials/analysis tools: AH AS CA MT DC KO RF UG JP.

26 Wrote the paper: AH AS DC UG JP.

27

28 **Competing Interests**

29 The authors declare that no competing interests exist.

30

31 **ABSTRACT**

32 Inflammatory control is critical to recovery from respiratory viral infection. Acetylcholine (ACh) secreted from
33 non-neuronal sources, including lymphocytes, plays an important, albeit underappreciated, role in regulating
34 immune-mediated inflammation. This study was designed to explore the role of ACh in acute viral infection and
35 recovery. Using the murine model of influenza A, cholinergic status in the lungs and airway was examined
36 over the course of infection and recovery. The results showed that airway ACh remained constant through the
37 early stage of infection and increased during the peak of the acquired immune response. As the concentration
38 of ACh increased, cholinergic lymphocytes appeared in the airway and lungs. Cholinergic capacity was found
39 primarily in CD4 T cells, but also in B cells and CD8 T cells. The cholinergic CD4+ T cells bound to influenza-
40 specific tetramers at the same frequency as their conventional (i.e., non-cholinergic) counterparts. In addition,
41 they were retained in the lungs throughout the recovery phase and could still be detected in the resident
42 memory regions of the lung up to two months after infection. Histologically, cholinergic lymphocytes were found
43 in direct physical contact with activated macrophages throughout the lung. When ACh production was
44 inhibited, mice exhibited increased tissue inflammation, altered lung architecture, and delayed recovery.
45 Together, these findings point to a previously unrecognized role for ACh in the transition from active immunity
46 to recovery and pulmonary repair following respiratory viral infection.

47 Introduction

48 A growing body of research indicates that acetylcholine (ACh) produced by specialized lymphocytes
49 plays a critical role in regulating inflammation and immunity(1-6). It is now understood that roughly 60% of the
50 ACh content of whole blood is sequestered within mononuclear leukocytes (MNLs), a group comprised of
51 mostly lymphocytes and a small number of monocytes(5-8). Immune cells preform and store ACh in a similar
52 fashion to neurons(9), allowing for quick and efficient release following appropriate stimulation. Modulation of
53 immune inflammatory responses by ACh occurs in a site and target specific manner(10). Vagal nerve derived
54 norepinephrine (NE) induces ACh release from cholinergic CD4⁺ T cells in the spleen, whereas cholinergic B-1
55 cells in the peritoneal cavity release ACh in response to TLR agonists, surface Ig ligation, and cholecystikinin
56 (CCK) (11, 12). During chronic hepatitis, both CD4 and CD8 cells secrete ACh in response to IL-21 (13).

57 ACh decreases inflammation in large part by action on local macrophages. Signal transduction via the
58 alpha-7 nicotinic ACh receptor ($\alpha 7$ -nAChR) decreases nuclear translocation of the Nf- κ B transcription factor,
59 ultimately reducing macrophage production of the pro-inflammatory cytokine TNF (10, 14). Ligation of $\alpha 7$ -
60 nAChR significantly reduces lung injury and overall mortality in septic shock models (14, 15). In addition, pro-
61 inflammatory cytokines TNF, IFN- γ , and IL-6 are increased in mice lacking the $\alpha 7$ -nAChR, further indicating
62 that $\alpha 7$ -nAChRs play a critical role in regulating macrophage-associated inflammation (16).

63 Efficient inflammatory regulation is a crucial feature of recovery from respiratory viral infection (17).
64 Overwhelming inflammation during viral illness, commonly called a “cytokine storm” results in significant lung
65 damage and greatly increased risk of death. This is well established for influenza as well as the novel
66 coronavirus COVID-19 (18, 19). Conversely, the decreased ability to properly induce and regulate inflammation
67 displayed by the elderly is also associated with increased overall morbidity and mortality from respiratory
68 infection (19-21).

69 This study was designed to explore the role of ACh during respiratory infection. Our results show that
70 the airway ACh concentration changes over the course of infection, and that the changes are mirrored by an
71 influx of cholinergic lymphocytes. Inhibiting ACh synthesis resulted in extended pulmonary inflammation,
72 increased macrophage activation, and delayed tissue repair. These findings illuminate a previously unknown
73 role of ACh in recovery from acute viral infection, and further illuminate the non-neuronal cholinergic system as
74 an underappreciated therapeutic target for inflammatory regulation, particularly during viral infection (22-24).

75 **Methods**

76
77 **Ethics Statement:** All animal experimental protocols were approved by the Institutional Animal Care and Use
78 Committee at San Diego State University (protocol numbers 15-06-006) and 18-06-008P) prior to initiation of
79 experiments. Animals were given free access to food and water at all times and were cared for according to
80 guidelines set by the American Association for Laboratory Animal Care.

81
82 **Animal Experimentation:** Conventional C57BL/6 and ChAT (BAC) – eGFP transgenic mice [B6.Cg-Tg(RP23-
83 268L19-EGFP)2Mik/J] with endogenous choline acetyltransferase (ChAT) transcriptional regulatory elements
84 directing eGFP expression were originally obtained from The Jackson Laboratory (JAX, Bar Harbor, ME) and
85 were bred in house. Animals were used between the ages of aged 12-20 weeks. Mice were infected with the
86 mouse adapted influenza virus A/Puerto Rico/8/34 (H1N1) (PR8) (Charles River Laboratories Avian Vaccine
87 Services, North Franklin, CT) delivered in a volume of 30 μ l exactly as in(25). All animals were examined for
88 overt indications of morbidity and weighed daily starting the day of infection. For euthanasia, animals were
89 exposed to isofluorane until respiration ceased. Death was confirmed by severing the abdominal aorta. For
90 inhibition of ACh synthesis, Hemicholinium-3 (HC3) (Millipore Sigma, Burlington, MA) was administered via
91 intraperitoneal (IP) injection. Animals were treated daily for six days, beginning seven days post infection (dpi).
92 Each animal was administered 100 μ L of a 10 μ g/mL HC3 solution dissolved in PBS for a final dose of 1 μ g of
93 HC3 daily. Control animals were administered 100 μ L of sterile PBS by IP injection on the same days.

94
95 **Flow Cytometry:** Following euthanasia, lungs were lavaged with 1 mL of sterile PBS as in in [Sanderson,
96 2012 #696]. Airway cell counts were immediately collected using an Accuri C6 flow cytometer (Accuri
97 Cytometers, Ann Arbor, MI) prior to centrifugation and separation of the airway cell pellet from the cell free
98 bronchial alveolar lavage (BAL) fluid. Lungs were removed, processed, and stained for flow cytometry as in
99 [Sanderson, 2012 #696]. Flow cytometry antibodies used in this study were: 1A8-FITC (BD PharMingen, San
100 Jose, CA), CD4-APC,, CD8-PE/Cy5, B220-PE (eBioScience, San Diego, CA) , CD11b-APC (BioLegend, San
101 Diego, CA), CD11c-PE/Cy5 (Tonbo Bioscience, San Diego, CA). To examine influenza specificity, lung and
102 airway lymphocytes were stained using the influenza-specific CD4 tetramer: I-A(b) Influenza A NP 311-325

103 QVYSLIRPNENPAHK as described(26). Negative control CD4 tetramer was I-A(b) human CLIP 87-101
104 PVSKMRMATPLLMQA. Tetramers were obtained from the NIH Tetramer Core Facility. Samples were
105 incubated with tetramer for 60 minutes at room temperature. For all flow cytometric studies, data acquisition
106 and analysis were performed on an Accuri C6 (BD Biosciences, San Jose, CA) flow cytometer using CFlow
107 Plus Analysis software.

108

109 **Mass Spectrometry:** Choline and ACh were measured in cell-free BAL fluid by hydrophilic interaction liquid
110 chromatography coupled to tandem mass spectrometry (HILIC LC–MS/MS), using stable isotope-labeled
111 internal standards (choline-d4 and acetylcholine-d4) as described (27, 28). Briefly, an aliquot of the cell-free
112 BAL fluid was spiked with a mixture of deuterated choline/deuterated ACh. The sample was adjusted to 50%
113 methanol and ice partitioned to remove proteins. The remaining sample was lyophilized, dissolved in
114 acetonitrile:H2O and analyzed using a Thermo-Finnigan TSQ Quantum LC-MS/MS in positive ion ESI mode.
115 For quantification, MS/MS ion transitions m/z 104 to 60 (choline), 108 to 60 (choline -d4), m/z 146 to 87 (ACh),
116 and 150 to 91(ACh-d4) were used.

117

118 **Histology:** Following euthanasia, exsanguination, and cannulation of the trachea, lungs were inflated with 1mL
119 of a 4% paraformaldehyde solution. The trachea was clamped and all lungs were removed and fully
120 submerged in the 4% paraformaldehyde solution overnight fixation (~18 hour), with hemostats still attached
121 and fully restricting flow through the trachea. The following day, hemostats were removed, lung lobes were
122 dissected from one another and fully submerged in 70% Ethanol (EtOH), which was replaced 6-8 hours. One
123 day prior to processing, EtOH was discarded and replaced for a further 24 hours before being sent for
124 processing and paraffin embedding. Formalin fixed paraffin embedded (FFPE) lung lobes were serially
125 sectioned at 5um on a Leica RM2125 RTS Rotary Microtome, and mounted on Prism (Prism Research Glass,
126 Raleigh, NC) positively charged microscope slides. Formalin fixed paraffin-embedded (FFPE) sections were
127 stained with Hematoxylin and Eosin (H&E) for histological analysis using standard methods. Tissue sections of
128 uninfected, infected vehicle control, and infected HC3 treated lung tissue were analyzed by a veterinary
129 pathologist who was blinded to treatments and groups.

130 For immunofluorescence studies, FFPE sections were deparaffinized and treated for
131 immunofluorescent imaging by standardized methods(29). Sections were blocked with a 10% normal goat
132 serum (NGS) solution for 30 minutes and incubated with primary antibody overnight at 4°C. All antibody
133 dilutions were made in a 2% normal goat serum solution. Detection of GFP and Iba1 required high-
134 temperature antigen unmasking in 0.01 M citrate buffer (pH 6.0) (Sigma-Aldrich, San Diego, CA). Sections
135 were treated with biotin and streptavidin blocking solutions (Vector Laboratories, Burlingame, CA) before
136 incubation with primary antibodies. Sections were incubated with a rabbit primary monoclonal antibody against
137 Iba1 [ionized calcium-binding adapter molecule 1 (Iba1): polyclonal rabbit anti-Iba1 antibody; Wako Pure
138 Chemicals Industries, Ltd, Osaka Japan] at 1:500 at 4C overnight. A goat secondary antibody [goat
139 biotinylated anti-rabbit IgG (H+L); Vector Laboratories, Burlingame, CA] at 1:500 was diluted in 2% normal
140 goat serum and incubated on sections for 30 minutes. After staining with secondary antibodies, all sections
141 were washed three times with phosphate buffered saline and incubated with a streptavidin-AlexaFluor 594
142 complex [DyLight 594 streptavidin conjugate; Vector Laboratories, Burlingame, CA] 1:500 diluted in 2% normal
143 goat serum. For tri-color stained sections, sections were incubated for 30 minutes in a light free environment
144 with an anti-GFP AlexaFluor-488 conjugate [anti-GFP, rabbit polyclonal antibody, Alexa Fluor 488 conjugate;
145 Invitrogen, Eugene, OR] diluted 1:5 in 2% normal goat serum. Specificity controls for immunostaining included
146 sections stained in the absence of primary antibody or in the presence of rabbit immunoglobulin G control
147 antibody at 0.1 ug/mL (Vector Laboratories, Inc.). Sections were overlaid with Vectashield anti-fade mounting
148 medium (Vector Laboratories, Burlingame, CA) containing DAPI (4', 6-diamidino-2phenylindole) to detect
149 DNA/nuclei (blue) and covered with glass coverslips. Sections were observed by fluorescence microscopy
150 (Zeiss Axio Observer D1 Inverted Phase Contrast Fluorescent Microscope). Green, red, and blue channel
151 images were merged using AxioVision software. Broad field images were taken on a Zeiss Axio Zoom.V16
152 Stereo Zoom Microscope (Zeiss, Germany).

154 **Automated Image Segmentation and Quantification of Immunofluorescence**

155 For regional comparison of the lungs between treatment groups, images were categorized into three
156 categories based on anatomical region: open alveolar space (open), bronchus associated lymphoid tissue
157 (BALT), and area peripheral to large airways (peri-bronchial). All images to be quantified were captured on a

158 Ziess Axio Observer D1 Inverted Phase Contrast Fluorescent Microscope at the same magnification, utilizing
159 the 20x objective with a digital zoom of 0.97. Exposure times were held constant in red, green, and blue
160 channels for each image captured, although only the signal in the red channel was quantified, as Iba1 was
161 marked with the AlexaFluor 594 fluorochrome. Exposure times were: red (2.1s), green (2.1s), blue (200ms).
162 The same exposure time was utilized for both the red and green channels for comparison of auto fluorescent
163 tissues within each section, such as red blood cells and fibrin deposits, commonly seen as a result of vascular
164 leakage in inflamed tissues. For Iba1 immunofluorescence quantification, only images in the red channel were
165 analyzed.

166
167 **Automated Image Segmentation:** A novel automated algorithm was designed and implemented in MATLAB
168 2019b Image Processing Toolbox to accurately quantifying the red stains present in the lungs. The program
169 locates and segments regions of interest while simultaneously calculating the size and intensity of these
170 regions. With a goal of capturing the red stain present in the images, the gray-scale red channel portion of the
171 original microscopy images were used for the automated image analysis process. The program follows three
172 main steps: image input, image segmentation, and data extraction. The step for the image input was
173 automated for efficiency by directing the program to read multiple images in a folder sequentially. After an
174 image is read, the program segments the red dots using Otsu's thresholding method in which background
175 noise in the image is eliminated by selecting a threshold automatically from a gray level histogram using
176 discriminant analysis(30). While there are a variety of thresholding methods present in the literature, Otsu's
177 method is the most accurate and most widely used(31-34). In the program, Otsu's method determines a
178 threshold that distinguishes the background from the region of interest. The determined threshold is then used
179 to segment each image, removing background noise and displaying the red stain. The final step is the
180 calculation of the total area of red stain present in the image as well as the intensity of the stains. Total pixel
181 area of red stain coverage is calculated by determining the number of nonzero elements in the gray scale
182 image while total image intensity is calculated by summing the intensity levels of all elements remaining in the
183 segmented image. The program analyzed all the microscopy images and generated graphs for total area of red
184 dots and intensity in approximately 29.6 seconds.

186 **Statistical Analysis:** Statistical analysis was computed using R and R Studio. One-way ANOVA and two-
187 tailed paired t-tests were performed *, $p < 0.05$ was considered statistically significant.

188

189 Results

190 Airway choline changes during infection and recovery

191 Animals were infected with a sublethal dose of influenza A/PR8 (H1N1) and weighed daily to monitor
192 morbidity (Fig 1A). Separate cohorts were euthanized at specified time points and BAL fluid was isolated in
193 order to measure the airway ACh concentration. Airway choline concentration was also measured as a
194 biomarker for local ACh hydrolysis(23). There was no change in the airway ACh concentration over time;
195 however, the airway choline concentration changed over the course of infection. From a background
196 concentration of 1200ng/ml prior to infection, the airway choline concentration increased to 4800 ng/mL 8 dpi
197 and peaked at 6500 ng/mL 10 dpi. By 15 dpi, BAL choline concentration diminished to 1800 ng/mL, similar to
198 the starting concentration measured 0 dpi (Fig 1B). Comparing the weight change curve to the choline
199 concentration changes shows that ACh hydrolysis reaches a peak in the influenza-infected lungs shortly after
200 the point of peak weight loss.

201 To determine the source of airway ACh and examine a possible role for non-neuronal ACh production
202 during influenza infection, we examined the kinetics of lymphocyte populations infiltrating airways and lungs
203 during infection using ChAT (BAC) – eGFP transgenic mice (ChAT mice) with endogenous choline
204 acetyltransferase transcriptional regulatory elements directing eGFP expression, alongside C57BL/6 mice as
205 non-reporter controls. Wild-type, influenza-infected C57BL/6 mice were used as controls for green fluorescent
206 protein (GFP) fluorescence. Starting 8 dpi, GFP⁺ cells were detected in the airway of the ChAT mice (Fig 1C).
207 The number of ChAT-GFP⁺ lymphocytes present in BAL samples followed the same kinetic pattern as the total
208 lymphocyte population (Fig 1D), increasing rapidly starting 7 dpi and reaching peak numbers between 8-10 dpi
209 (Fig 1E). However, the percentage of ChAT-GFP⁺ lymphocytes remained above 7% of the total lymphocyte
210 population in the airways through 28 dpi (Fig 1F).

211 **Figure 1: Cholinergic status kinetics in the influenza-infected Lung.**

212 *Mice were infected with a non-lethal dose of influenza (0.336MLD50) as described in Materials and Methods.*
213 *Mice were weighed daily starting the day of infection. A. Weight change following influenza infection. Group*
214 *average weight change is shown as mean ± SEM. B. Airway choline concentration was measured using HILIC*
215 *LC–MS/MS with a stable choline-d4 isotope-labeled internal standard as described in Materials and Methods.*
216 *C. Ten dpi, airway cells were isolated by lung lavage, stained with fluorescent antibodies and analyzed by*

217 *FACS as described in Materials and Methods. FACS plots shown are from individual mice representative of at*
218 *least 10 mice per time point. Gating strategy for BAL cell analysis is shown using wild-type C57Bl/6 mouse as*
219 *a negative control for GFP fluorescence. Representative staining data is shown (10–30 mice per time point).*
220 *FSC: forward scatter (size); SSC: side scatter. Cholinergic capacity was defined as increased FL1*
221 *fluorescence compared to wild-type C57Bl/6. D. Kinetics of total airway lymphocytes; E. Kinetics of airway*
222 *cholinergic (GFP⁺) cells; F. Percentage of all lymphocytes expressing GFP over the course of influenza*
223 *infection.*

224
225 Flow cytometry identified ChAT-GFP⁺ subsets of both CD4⁺ and CD8⁺ T cell populations in the airways
226 during peak days of infection (8-10 dpi) (Fig 2). The majority of these ChAT-GFP⁺ lymphocytes were CD4⁺
227 (69.7%) while 23.3% were CD8⁺, indicating more cholinergic helper T cells present in BALF samples than
228 cholinergic cytotoxic T cells, respectively. When the analysis was extended to lung tissue, ChAT-GFP was
229 detected in B220⁺ B-1 lymphocytes as well as CD4 and CD8 T cells. In airway and lung tissue, the highest
230 percentage of GFP⁺ cells were CD4⁺ T cells. The CD4 population also expressed the most GFP fluorescence
231 on a per-cell basis (Table 1).

232 233 **Figure 2. Airway and Lung Cholinergic Cell Phenotyping**

234 *Animals were infected with influenza and sacrificed ten days later. Cells were isolated and stained for surface*
235 *marker analysis as described in Materials and Methods. Gating strategy to examine surface phenotypes of FL-*
236 *1⁺ and FL-1⁻ cells is shown.*

245 **Table 1. Pulmonary Cholinergic Lymphocyte Phenotype**

	% ChAT-GFP	ChAT-GFP MFI
BAL CD4	26 + 1	21423 + 2127
Lung CD4	21 + 2	21278 + 2110
BAL CD8	6 + 2	7893 + 3222
Lung CD8	4 + 1	9972 + 3324
Lung B220	11 + 2	13749 + 1393

246

247 *Day 10 post infection. Data compiled from five experiments, mean ± SE*

248

249 Influenza antigen specificity of the TCR in cholinergic and conventional T cell populations was
250 examined by tetramer staining (Fig 3). Neither conventional nor cholinergic CD4 T cells bound to fluorescent
251 tetramers loaded with negative control peptide (human CLIP 87-101). Similar percentages of cholinergic CD4
252 T cells and conventional T cells bound the dominant influenza A epitope NP311-325 (Fig 3).

253

254 **Figure 3. Cholinergic CD4 T cells bind to influenza-specific tetramers**

255 *Mice were infected with influenza A/PR8 and sacrificed for analysis 8 days later. BAL cells were isolated and*
256 *stained the anti-CD4 as in figure 2. Cells were then stained with either the class II tetramer I-A(b) Influenza A*
257 *NP 311-325 (top) or the negative control tetramer I-A(b) human CLIP 87-101 (bottom). Histograms show*
258 *staining of either R1 = conventional CD4 T cells; R2 = cholinergic CD4 T cells vs. ChAT-GFP fluorescence.*

259

260 Surface staining indicated that the cholinergic CD4 T cells were uniformly CD44^{hi}CD62L^{lo} (Fig 4). This
261 matches the overall surface phenotype of cholinergic CD4 T cells from multiple reports, but it also corresponds
262 with a specific subset associated with long term memory known as the T resident memory population. To
263 explore the possibility that cholinergic CD4 T cells made up part of the TRM population, mice were infected
264 with influenza A and allowed to recover for two months with no manipulation, then they were given an
265 intravenous injection of fluorescent anti-CD45 antibody and sacrificed ten minutes later. As shown in Fig 4B,
266 CD4 positive cells in the lungs can be divided into two subsets, based on staining by the injected CD45. Those
267 cells not exposed to the circulation were left unstained following iv injection. These represent the T resident
268 memory (TRM) population. The T effector memory (TEM) reside in areas of the lung accessible to the

269 circulation and were stained following iv injection of fluorescent antibody(35). Cholinergic CD4 T cells were
270 primarily found in the regions of the lung sequestered from circulation, associated with the TRM population (Fig
271 4B).

272 **Figure 4. Cholinergic CD4 T cells reside in the resident memory niche of the lung.** *Two months after*
273 *influenza infection, mice were injected intravenously with fluorescent anti-CD45 ten minutes before sacrifice.*
274 *Lung lymphocytes were stained for surface markers and analyzed based on GFP expression as in Figures 1*
275 *and 2. A. Gated CD4 cells were stained for memory markers CD44 and CD62L. B. Total lymphocytes from*
276 *ChAT-GFP mice were analyzed based on fluorescence of the infected CD45 antibody vs CD4 expression. CD4*
277 *positive populations were then analyzed for GFP expression.*

278

279 **Cholinergic Lymphocytes associate with activated macrophages**

280 To explore the localization of cholinergic cells within the context of the overall lung architecture, lungs from
281 animals infected with influenza A were fixed and processed for immunofluorescent (IF) staining and analysis.
282 Cholinergic cells were identified by staining with an anti-GFP fluorescent antibody. The cholinergic GFP⁺ cells
283 were predominantly localized to bronchus associated lymphoid tissues (BALT) but they were also observed in
284 open spaces, specifically the alveolar space and peri-bronchial regions proximal to the major sites of active
285 inflammation or infection, identified by Iba1 staining. Iba1, also known as allograft inflammatory factor 1 or AIF-
286 1, is a marker of activated macrophages and ongoing inflammation(8, 29, 36-38). As shown in Fig 5,
287 cholinergic lymphocytes were regularly observed in direct physical contact or close spatial proximity with Iba1⁺
288 activated macrophages. Co-expression of ChAT-GFP and Iba1 was never observed within the same cell in
289 vehicle control or HC3 treated lungs.

290

291 **Figure 5. Cholinergic lymphocytes are found in direct contact with activated macrophages throughout the**
292 **lung.** *Dual labeled sections (Green: ChAT-GFP, Red : Iba1) of infected vehicle control and HC3 treated lungs*
293 *from 12 dpi show close contact of cholinergic lymphocytes (ChAT-GFP⁺) and activated macrophages*
294 *(Iba1⁺). Alveolar space and Peri-bronchial region images captured at 63x oil immersion with 1.4x digital*
295 *zoom. BALT image captured at 40x oil immersion with 1.3x digital zoom. Arrows point out areas of*
296 *lymphocyte-macrophage contact.*

297

298 **Blocking ACh synthesis increases viral-associated morbidity**

299 The co-localization of cholinergic lymphocytes and activated macrophages indicated a potential role for
300 targeted ACh delivery to activated macrophages during the later stages of influenza infection. To examine the
301 requirement for ACh during recovery from influenza infection, we used the choline reuptake inhibitor
302 Hemicholinium-3 (HC3) to disrupt ACh synthesis during the time period associated with the increased airway
303 ACh concentration (Fig 1). Mice were infected with influenza A/PR8 (H1N1) as above. After seven days, mice
304 were stratified into treatment cohorts according to the amount of weight loss to ensure equivalent pre-
305 established morbidity in each cohort. One cohort was treated with HC3 from days 7 through 12 (infected HC3
306 treated), while the infected vehicle control cohort was injected with saline to control for handling/injection
307 stress. Additional control cohorts were injected with HC3 or PBS without having been infected. One infection
308 cohort was sacrificed 10 dpi to measure the airway choline concentration. BAL samples from the HC3 treated
309 cohort exhibited increased airway choline concentration compared to infected vehicle control groups, indicating
310 that HC3 was inhibiting choline uptake in the pulmonary airways (Fig 6A). All influenza infected cohorts lost
311 weight as expected. The infected control cohort began to regain weight 9 dpi and had returned to 96% of their
312 starting weight by 15 dpi. In contrast, the infected HC3 treated cohort did not begin to regain weight until 11 dpi
313 and only returned to 91% of their starting weight by 15 dpi. The uninfected cohort treated with HC3 did not
314 display any treatment-associated weight change (Fig 6B). Flow cytometric analysis showed an increase in the
315 number of neutrophils in HC3 treated animals compared to vehicle control animals (Fig 6C).

316

317 **Figure 6. Decreasing ACh synthesis delays recovery and increases inflammation following influenza**
318 **infection.** Mice were infected with influenza and injected with HC3 or PBS 7-12 dpi as described in Materials
319 and Methods. **A.** Airway choline was measured ten days after infection as in Figure 1. **B.** Weight was
320 measured daily throughout infection and recovery. Control cohorts were injected with either HC3 or PBS but
321 were not infected with influenza. Group average weight changes are shown as mean \pm SEM. **C.** On days 10
322 and 15 after infection, pulmonary neutrophils (SSC^{hi}CD11b⁺Ly6G/1A8⁺) in the influenza-infected cohorts were
323 identified by FACS analysis.

324

325 **Blocking Ach synthesis increases pulmonary inflammation**

326 We used Iba1 as a marker of overall inflammation(8, 29, 36-38) to determine the effect of HC3
327 treatment during the later stage of infection (Fig 7). Fluorescent signal from immunofluorescence stained
328 slides was quantified spatially to determine the degree of inflammation at set time points. A novel automated
329 algorithm was designed and implemented in MATLAB 2019b Image Processing Toolbox to accurately
330 quantifying the red stains present in the lungs. The program locates and segments regions of interest while
331 simultaneously calculating the size and intensity of these regions, using Otsu's method of thresholding in order
332 to remove background noise and isolate the red stain with minimal human bias(30, 32-34). Area of stain, which
333 corresponds to the total number of pixels occupied by fluorescent signal from any one image, was evaluated
334 by region and compared between infected HC3 treated groups and infected vehicle control groups. Area of
335 stain from Iba1 fluorescence differed between regions of the lung in both HC3 treated animals and vehicle
336 control animals (Fig 7B). Area of stain measurements from infected HC3 treated groups were greater than
337 those observed in infected vehicle control groups in all three lung regions, as well as tissue wide. Total
338 intensity, corresponding to the sum of fluorescent stain intensity per pixel in one image, was measured by an
339 novel automated image segmentation algorithm and evaluated by region and compared between influenza-
340 infected HC3 treated vs. vehicle control groups (Fig 7C). Total intensity was determined to be greater in
341 infected HC3 treated groups compared to infected vehicle control groups in all three lung regions, as well as
342 tissue wide.

343 **Figure 7: IHC Analysis of Iba1 During Recovery** *A. Immunofluorescence of Iba1 staining in multiple lung regions 15dpi.*
344 *Representative images taken at 20x showing Iba1 staining (red, AlexaFluor-594) and DAPI stained nuclei (blue) in the*
345 *alveolar space, peri-bronchial region, and bronchus associated lymphoid tissues (BALT) in uninfected, infected vehicle*
346 *control, and infected drug treated animals 15 dpi. Increased intensity and area of stain was observed in all lung regions*
347 *of infected HC3 treated groups when compared to infected vehicle control groups. B. Quantification of Iba1 staining in*
348 *HC3 and Control animal immunofluorescence sections. Area of stain analysis indicated more numerous pixels occupied*
349 *by fluorescent signal in the lungs of infected HC3 treated groups compared to infected vehicle control groups in all three*
350 *lung regions individually. Area of stain was also greater in infected HC3 treated groups compared to infected vehicle*
351 *control groups when measurements of three lung regions were combined into a single data set. C. Total intensity*
352 *analysis identified greater total intensity of fluorescent signal in the lungs of infected HC3 treated groups compared to*

353 *infected vehicle control groups in the alveolar space and peri-bronchial regions, as well as the full lung when all*
354 *measurements were compiled into a single data set. Greater total fluorescent intensity was also observed in the BALT*
355 *region of infected HC3 treated groups compared to infected vehicle control groups, but was less significant than other*
356 *regions or tissue wide.*

358 **Decreasing Ach results in increased lung pathology**

359 Lung samples from the HC3-treated animals and controls were collected 15 dpi, fixed and processed
360 for staining examined to determine the effect of ACh disruption on tissue repair. As shown in Fig 8, infected
361 vehicle control lung tissue was characterized by having mild/moderate multifocal perivascular mixed infiltrate
362 and alveolar/interstitial mixed infiltrate of lymphocytes and neutrophils. However, infected HC3 treated lung
363 tissue exhibited histological abnormalities not seen in the vehicle control lungs. The lungs from infected
364 animals treated with HC3 were characterized as having moderate perivascular as well as alveolar/interstitial
365 mixed infiltrate of lymphocytes and neutrophils (Fig 8A). In addition, pathological anomalies including as
366 multifocal type II pneumocyte proliferation (Fig 8B), mild multifocal squamous cell metaplasia (Fig 8C), and
367 mild fibroplasia (Fig 8D) were observed in infected HC3 treated lung tissue but were absent in infected vehicle
368 control lung tissue.

370 **Figure 8: Histological Analysis of Recovery**

371 *A. Representative images of H&E stained sections of lung tissue at 10x (scale bar 100um) and 40x (scale bar*
372 *10um) magnification from healthy animals, infected vehicle control animals, and infected HC3 treated animals*
373 *from left to right. Flu infected vehicle control lung tissue with mild/moderate multifocal perivascular mixed*
374 *infiltrate (yellow arrow) and alveolar/interstitial mixed infiltrate of lymphocytes and neutrophils (green arrow).*
375 *Flu infected HC3 treated lung tissue with moderate perivascular (yellow arrows) as well as alveolar/interstitial*
376 *mixed infiltrate of lymphocytes and neutrophils (green arrows). B-D. Infected HC3 treated lung tissue shows*
377 *multifocal type 2 pneumocyte proliferation (yellow arrows), mild multifocal squamous cell metaplasia (green*
378 *arrows), and mild fibroplasia (blue arrows).*

379 Discussion:

380 The present study adds to a growing body of research illuminating the crucial role of non-neuronal ACh
381 in regulating inflammation and immunity. Our results demonstrate that ACh plays an important role in recovery
382 from pulmonary viral infection. Inflammatory control and pulmonary tissue repair is critically important during
383 respiratory infection, especially in the alveolar space where the majority of gas exchange occurs. Disruption of
384 the delicate architecture of the alveolar space by direct viral damage and inflammatory cell influx during
385 infection results in significant reduced tidal volume and a decreased capacity for gas exchange.

386 These studies used influenza A; however, the results are likely to be applicable to many acute
387 respiratory infections including the pandemic SARS-CoV coronavirus COVID-19. As widely observed during
388 the yearly influenza season as well as the current COVID-19 pandemic, many patients in critical condition
389 exhibit significantly reduced tidal volume and capacity for gas exchange, resulting in the critical need for
390 ventilators worldwide. Our findings that ACh from cholinergic lymphocytes regulates pulmonary inflammation
391 and plays a role in tissue repair point to a previously unexploited therapeutic target for treating respiratory
392 infection.

393 Based on previously published studies demonstrating ACh regulating inflammatory cytokine
394 expression, macrophage activation, and neutrophil trafficking(11, 12, 14, 39-43), we initially hypothesized that
395 ACh would modulate the innate immune burst at the earliest the early stages of respiratory viral infection.
396 However, we found no evidence increased cholinergic activity during the first week of influenza infection.
397 Although other studies have demonstrated ChAT expression in natural killer cells and myeloid populations(44),
398 we could not unequivocally identify ChAT expression in NK cells, myeloid cells, or alveolar macrophages at
399 any state of infection. Instead we determined that the peak concentration of airway ACh mirrored the kinetics
400 of the airway CD4 T cell population, between 8-10 days after infection. These findings suggested a role in
401 regulating the cellular immune response and/or the transition from active immunity to tissue repair rather than
402 modulating the innate immune burst. Further supporting a role in recovery and repair, cholinergic lymphocyte
403 numbers did not increase during the innate response, but they were retained in the airway and lungs
404 throughout the late stages of infection and long after clinical recovery. Data shown here indicates that
405 cholinergic CD4 T cells are present for at least two months after recovery, well past the time point associated
406 with establishment of the CD4 T cell resident memory population(35, 45). The long-term retention of

407 cholinergic CD4 T cells in the circulation-sequestered niche of the lung, along with their surface phenotype of
408 CD44^{hi}CD62L^{lo}, lead to speculation that they may also play an important role in the memory T cell response.
409 Since expression of the ChAT-eGFP gene is transient, the ChAT mice used herein cannot be used to
410 determine the full percentage of cells with a cholinergic history. The use of lineage tracer animals will be
411 necessary to fully address these questions.

412 Despite the clear influx of cholinergic lymphocytes and increased airway choline concentration, we
413 were unable to detect changes in the airway ACh concentration. This is consistent with other studies in the
414 lung(42). The in vivo half-life of ACh is extremely short due to the efficiency of the specific enzymes
415 acetylcholinesterase (AChE) and butyrylcholinesterase (BuChE)(46). To overcome this rapid degradation,
416 cholinergic signaling between cells must take place over a relatively short distance. We found evidence of
417 direct physical contact between Iba1⁺ macrophages and cholinergic lymphocytes in the influenza-infected lung.
418 This contact illustrates a biologic method to ensure proper targeting of the secreted ACh while overcoming the
419 rapid ACh hydrolysis in the pulmonary environment. This direct physical interaction also offers a biological
420 explanation for the presence of cholinergic lymphocytes in a tissue that already possesses two endogenous
421 sources of ACh. The cholinergic vagal nerve can be detected in bronchus-associated lymphoid tissue but it
422 does not enervate the airway. Bronchial epithelium, which lines the airway, is also cholinergic. Our results
423 showed evidence of direct physical interaction between the cholinergic lymphocytes and activated
424 macrophages in all regions of the lungs. In the BALT and peri-bronchial lung regions, multiple sources of ACh
425 may contribute to cholinergic signaling whereas the alveolar space is relatively inaccessible to ACh secreted
426 by bronchial epithelium or the vagal nerve. In addition, although our studies did not determine the primary
427 inducers of ACh secretion by the cholinergic lymphocytes, previous studies have shown that cholinergic
428 lymphocytes produce ACh in response to specific antigen, TLR agonists, neurotransmitters, and cytokines (11-
429 13, 47). As yet we do not know if local neurotransmitter secretion plays any role in lymphocyte ACh production
430 during influenza. For this reason, we have not used the term cholinergic anti-inflammatory pathway, or CAP,
431 since we do not yet what role the brain-immune circuit plays in this process.

432 Although flow cytometry indicated that CD4 T cells were the dominant cholinergic population in
433 absolute numbers and per-cell ChAT expression, the fluorescent images do not confirm the identity of the
434 cholinergic cell population(s) seen in contact with pulmonary macrophages. The physical contact between

435 cholinergic lymphocytes and activated macrophages throughout the lungs provide evidence for the specialized
436 role of cholinergic lymphocytes as mediators of localized cholinergic signaling and offers a mechanism to avoid
437 deleterious consequences of increased ACh concentration.

438 The importance of ACh in recovery was indicated by the increased inflammation and aberrant tissue
439 repair noted when ACh synthesis was inhibited. These observations support a necessary, protective role for
440 ACh mediating anti-inflammatory and tissue repair oriented mechanisms in the late stages of infection. ACh as
441 a critical mediator of pulmonary repair following viral illness is consistent with other reports in the literature.
442 ACh increases proliferation of bronchial epithelium, whereas decreased ACh slows proliferation (48). Animals
443 with an endogenous defect in ACh generation exhibit abnormal lung remodeling even in the absence of overt
444 injury (49). Our findings are also supported by studies using different models of acute lung injury (i.e., acid,
445 LPS, *E. coli*), where injury is increased when cholinergic signaling is inhibited and decreased when it is
446 augmented(15, 42, 50).

447 In addition to inducing epithelial proliferation, ACh mediates changes in macrophage gene expression.
448 The anti-inflammatory activity of ACh binding to the $\alpha 7$ nAChR on macrophages, resulting in diminished NF- κ B
449 nuclear translocation and decreased inflammatory cytokine production is well described(39, 51) and has been
450 documented in the lungs(22, 42, 50). Recently, loss of $\alpha 7$ nAChR signal transduction was shown to decrease
451 expression of the canonical M2 marker Arginase-1(52). In addition, use of an $\alpha 7$ nAChR agonist decreased the
452 LPS-induced inflammatory response and reversed the inflammatory profile, particularly regarding M1 and M2
453 polarization, while also improving lung function and remodeling in a model of acute lung injury(15). Based on
454 these findings and those in the current study, we hypothesize that ACh produced by cholinergic lymphocytes
455 acts on $\alpha 7$ nAChR macrophages to decrease pro-inflammatory cytokine release and initiate tissue repair
456 during the recovery phase of respiratory viral infection.

457 In these studies, we used a novel analysis tool to quantify Iba1 expression, relating to pulmonary
458 inflammation. An automated MATLAB algorithm was implemented to accurately isolate the red stain in the
459 Iba1 fluorescent images. The algorithm automatically reads images from a folder sequentially, segments the
460 red stains and computes the amount of red stain present in each of the images. To perform the image
461 segmentation to isolate the red stain, Otsu's method of thresholding was implemented in order to remove
462 background noise with minimal human bias. The algorithm was automated for computational efficiency and

463 avoids the laborious process of manual segmentation and analysis. Using the algorithm, we investigated Iba1
464 expression during pulmonary inflammation in different regions of the lungs. The automated algorithm proved to
465 be a valuable tool to quantitate Iba1 expression of pulmonary inflammation, allowing for a quick and accurate
466 analysis of each image with minimal of human bias. The results indicated that Iba1 is involved in the
467 pathogenesis of respiratory viral infection. To the best of our knowledge, this is the first time that Iba1 has
468 been linked to pathology during viral infection. The increased Iba1 expression displayed by infected animals
469 treated with HC3 is also consistent with decreased ACh-induced inflammatory regulation. The histopathological
470 observations in these animals indicate a higher degree of ongoing inflammation when ACh synthesis is
471 pharmacologically disrupted. As an activation marker, Iba1 can be detected on alveolar macrophages as well
472 as myeloid-derived pulmonary macrophages(53). More cells expressed Iba1 in the infected, HC3 treated
473 animals, resulting in larger areas of immunofluorescence. These animals also displayed higher mean staining
474 intensity, indicating that overall Iba1 expression was increased following disruption of ACh synthesis during
475 infection. Although Iba1 has historically been used as an activated macrophage marker(53), the secreted Iba1
476 protein also acts as an independent inflammatory stimulus. IBA/AIF-1 induces IL-6, TNF α , and CXCL1 (KC)
477 production by pulmonary macrophages and fibroblasts(8, 36). The increased neutrophils in the HC3-treated
478 animals would be consistent with increased pulmonary CXCL1(54).

479 In the context of our study, we hypothesize that elevated expression of Iba1 following ACh disruption is
480 both indicative of and enhances the ongoing inflammation observed in the lungs. Although the overall role of
481 Iba1 in influenza pathogenesis remains to be elucidated, the overall increased inflammation and delayed
482 recovery in ACh-depleted animals shown here is reminiscent of the response seen in aged animals to
483 respiratory infection(55). Aging is well established as the primary risk factor in murine influenza, human
484 influenza, and currently in the COVID-19 pandemic. Aging also impacts multiple aspects of cholinergic
485 systems beyond expression and cellular distribution of the $\alpha 7nAChR$ changes with age, activity, and continued
486 exposure to ACh (reviewed in (56, 57). Aging alters the T lymphocyte response to cholinergic stimulation(58),
487 as well as immune system ACh generation(59, 60). If altered cholinergic capacity plays a role in the
488 diminished immune response or delayed recovery to respiratory infection shown by the elderly, then improving
489 cholinergic function could result in enhanced immune function during aging. Since the elderly are at the
490 greatest risk of death not just from influenza infection but also from the ongoing COVID-19 pandemic, these

491 are questions of the utmost importance. One key feature of age-related immunodeficiency is in the increased
492 basal inflammatory status known as inflammaging(61, 62). Supporting the concept of improving immunity in
493 through cholinergic manipulation, it was first shown over 15 years ago that treatment with the AChE antagonist
494 donepezil decreased inflammatory cytokine message in circulating blood leukocytes of Alzheimer's Disease
495 patients(63, 64). This study was only recently followed up with the demonstration that inflammatory cytokines
496 TNF, IFN γ , IL1b, and IL6 were significantly decreased following six months of donepezil therapy(65).
497 Furthermore, donepezil treatment is associated with decreased overall mortality, including pneumonia-
498 associated mortality (66, 67). As yet, these data are not available for COVID-19 patients. Given the critical
499 unmet need of the elderly for better therapeutic options, extended studies into improved immune function
500 through cholinergic manipulations are of the utmost importance from both a scientific and a world health
501 perspective.

503 **Summation:**

504 ACh has shown to be of extreme importance in recovery from influenza A viral infection. While further
505 studies are needed to elucidate the full mechanistic understanding, ACh has shown to be a critical factor in
506 post-influenza infection recovery. Cholinergic lymphocytes appear in the lungs and airways during the recovery
507 phase of influenza, and are found in direct physical contact with activated macrophages. Artificially decreasing
508 the airway ACh concentration results in extended morbidity, disordered tissue repair, and increased pulmonary
509 inflammation. Together, these results indicate a previously unsuspected role for ACh in mediating pulmonary
510 inflammation and efficient tissue repair during recovery from respiratory viral infection.

511

512

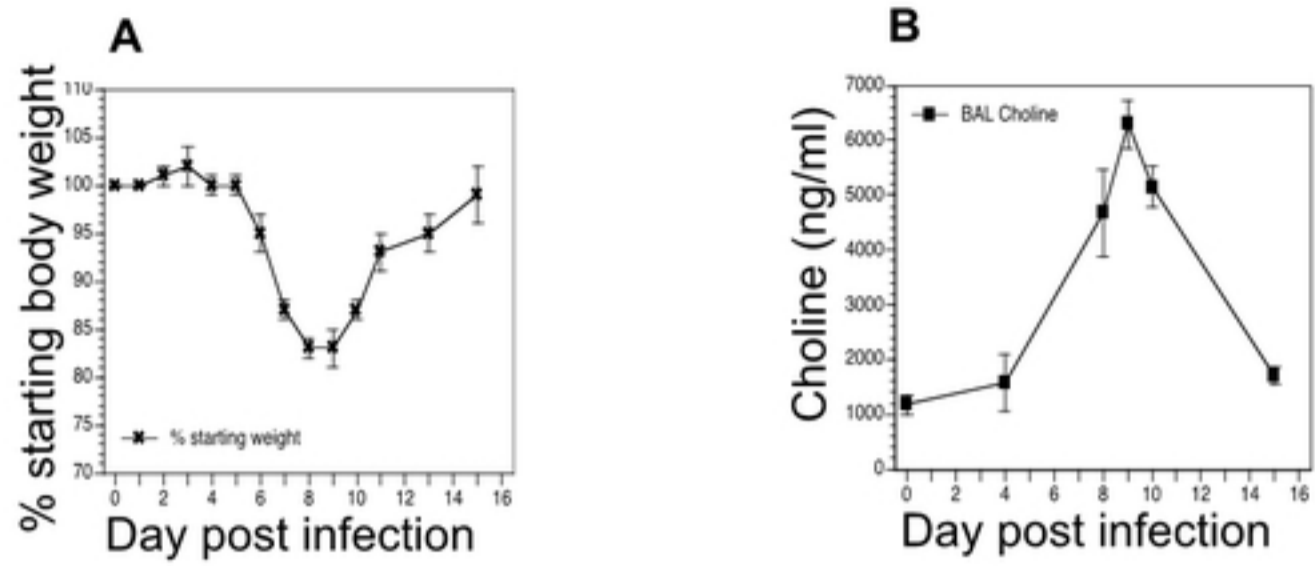
References:

- 513 1. Kawashima K, Oohata H, Fujimoto K, Suzuki T. Plasma concentration of acetylcholine in young women.
514 *Neurosci Lett*. 1987;80(3):339-42.
- 515 2. Kawashima K, Oohata H, Fujimoto K, Suzuki T. Extraneuronal localization of acetylcholine and its
516 release upon nicotinic stimulation in rabbits. *Neurosci Lett*. 1989;104(3):336-9.
- 517 3. Fujii T, Yamada S, Yamaguchi N, Fujimoto K, Suzuki T, Kawashima K. Species differences in the
518 concentration of acetylcholine, a neurotransmitter, in whole blood and plasma. *Neurosci Lett*.
519 1995;201(3):207-10.
- 520 4. Fujii T, Mori Y, Tominaga T, Hayasaka I, Kawashima K. Maintenance of constant blood acetylcholine
521 content before and after feeding in young chimpanzees. *Neurosci Lett*. 1997;227(1):21-4.
- 522 5. Kawashima K, Fujii T, Moriwaki Y, Misawa H, Horiguchi K. Non-neuronal cholinergic system in
523 regulation of immune function with a focus on $\alpha 7$ nAChRs. *Int Immunopharmacol*. 2015;29(1):127-34.
- 524 6. Fujii T, Mashimo M, Moriwaki Y, Misawa H, Ono S, Horiguchi K, et al. Expression and Function of the
525 Cholinergic System in Immune Cells. *Frontiers in Immunology*. 2017;8:1085.
- 526 7. Nosaka N, Yashiro M, Yamada M, Fujii Y, Tsukahara H, Liu K, et al. Anti-high mobility group box-1
527 monoclonal antibody treatment provides protection against influenza A virus (H1N1)-induced pneumonia in
528 mice. *Crit Care*. 2015;19:249.
- 529 8. Nagahara H, Yamamoto A, Seno T, Obayashi H, Kida T, Nakabayashi A, et al. Allograft inflammatory
530 factor-1 in the pathogenesis of bleomycin-induced acute lung injury. *Biosci Trends*. 2016;10(1):47-53.
- 531 9. Tayebati SK, El-Assouad D, Ricci A, Amenta F. Immunochemical and immunocytochemical
532 characterization of cholinergic markers in human peripheral blood lymphocytes. *J Neuroimmunol*. 2002;132(1-
533 2):147-55.
- 534 10. Cox MA, Bassi C, Saunders ME, Nechanitzky R, Morgado-Palacin I, Zheng C, et al. Beyond
535 neurotransmission: acetylcholine in immunity and inflammation. *J Intern Med*. 2020;287(2):120-33.
- 536 11. Rosas-Ballina M, Olofsson PS, Ochani M, Valdes-Ferrer SI, Levine YA, Reardon C, et al. Acetylcholine-
537 synthesizing T cells relay neural signals in a vagus nerve circuit. *Science*. 2011;334(6052):98-101.
- 538 12. Reardon C, Duncan GS, Brustle A, Brenner D, Tusche MW, Olofsson PS, et al. Lymphocyte-derived ACh
539 regulates local innate but not adaptive immunity. *Proc Natl Acad Sci U S A*. 2013;110(4):1410-5.
- 540 13. Cox MA, Duncan GS, Lin GHY, Steinberg BE, Yu LX, Brenner D, et al. Choline acetyltransferase-
541 expressing T cells are required to control chronic viral infection. *Science*. 2019;363(6427):639-44.
- 542 14. Wang H, Yu M, Ochani M, Amella CA, Tanovic M, Susarla S, et al. Nicotinic acetylcholine receptor
543 $\alpha 7$ subunit is an essential regulator of inflammation. *Nature*. 2003;421(6921):384-8.
- 544 15. Pinheiro NM, Santana FPR, Almeida RR, Guerreiro M, Martins MA, Caperuto LC, et al. Acute lung injury
545 is reduced by the $\alpha 7$ nAChR agonist PNU-282987 through changes in the macrophage profile. *The FASEB*
546 *Journal*. 2017;31(1):320-32.
- 547 16. Kawashima K, Yoshikawa K, Fujii YX, Moriwaki Y, Misawa H. Expression and function of genes encoding
548 cholinergic components in murine immune cells. *Life Sci*. 2007;80(24-25):2314-9.
- 549 17. Aghasafari P, George U, Pidaparti R. A review of inflammatory mechanism in airway diseases.
550 *Inflammation Research*. 2019;68(1):59-74.
- 551 18. D'Elia RV, Harrison K, Oyston PC, Lukaszewski RA, Clark GC. Targeting the "cytokine storm" for
552 therapeutic benefit. *Clin Vaccine Immunol*. 2013;20(3):319-27.
- 553 19. Zhang X, Tan Y, Ling Y, Lu G, Liu F, Yi Z, et al. Viral and host factors related to the clinical outcome of
554 COVID-19. *Nature*. 2020.
- 555 20. Eickhoff TC, Sherman IL, Serfling RE. Observations on excess mortality associated with epidemic
556 influenza. *Jama*. 1961;176:776-82.
- 557 21. McElhaney JE, Verschoor CP, Andrew MK, Haynes L, Kuchel GA, Pawelec G. The immune response to
558 influenza in older humans: beyond immune senescence. *Immun Ageing*. 2020;17:10.

- 559 22. Wessler IK, Kirkpatrick CJ. The Non-neuronal cholinergic system: an emerging drug target in the
560 airways. *Pulm Pharmacol Ther.* 2001;14(6):423-34.
- 561 23. Gwilt CR, Donnelly LE, Rogers DF. The non-neuronal cholinergic system in the airways: an
562 unappreciated regulatory role in pulmonary inflammation? *Pharmacol Ther.* 2007;115(2):208-22.
- 563 24. Grando SA, Kawashima K, Kirkpatrick CJ, Meurs H, Wessler I. The non-neuronal cholinergic system:
564 basic science, therapeutic implications and new perspectives. *Life Sci.* 2012;91(21-22):969-72.
- 565 25. Sanderson SD, Thoman ML, Kis K, Virts EL, Herrera EB, Widmann S, et al. Innate immune induction and
566 influenza protection elicited by a response-selective agonist of human C5a. *PLoS One.* 2012;7(7):e40303.
- 567 26. Scriba TJ, Purbhoo M, Day CL, Robinson N, Fidler S, Fox J, et al. Ultrasensitive detection and
568 phenotyping of CD4+ T cells with optimized HLA class II tetramer staining. *J Immunol.* 2005;175(10):6334-43.
- 569 27. Schebb NH, Fischer D, Hein EM, Hayen H, Krieglstein J, Klumpp S, et al. Fast sample preparation and
570 liquid chromatography-tandem mass spectrometry method for assaying cell lysate acetylcholine. *J Chromatogr*
571 *A.* 2008;1183(1-2):100-7.
- 572 28. Tufi S, Lamoree M, de Boer J, Leonards P. Simultaneous analysis of multiple neurotransmitters by
573 hydrophilic interaction liquid chromatography coupled to tandem mass spectrometry. *J Chromatogr A.*
574 2015;1395:79-87.
- 575 29. Feuer R, Ruller CM, An N, Tabor-Godwin JM, Rhoades RE, Maciejewski S, et al. Viral persistence and
576 chronic immunopathology in the adult central nervous system following Coxsackievirus infection during the
577 neonatal period. *J Virol.* 2009;83(18):9356-69.
- 578 30. Otsu N. A Threshold Selection Method from Gray-Level Histograms. *IEEE Trans Syst Man Cybern.*
579 1979;9(1):62-6.
- 580 31. Sahoo PK, Soltani S, Wong AKC. A survey of thresholding techniques. *Computer Vision, Graphics, and*
581 *Image Processing.* 1988;41(2):233-60.
- 582 32. Vala H, Baxi A. A review on Otsu image segmentation algorithm. *International Journal of Advanced*
583 *Research in Computer Engineering & Technology* 2013;2(2):387-9.
- 584 33. Mohammadi-Sardo S, Labibi F, Shafiei SA. A new approach for detecting abnormalities in
585 mammograms using a computer-aided windowing system based on Otsu's method. *Radiol Phys Technol.*
586 2019;12(2):178-84.
- 587 34. Xiao L, Ouyang H, Fan C, Umer T, Poonia RC, Wan S. Gesture image segmentation with Otsu's method
588 based on noise adaptive angle threshold. *Multimedia Tools and Applications.* 2020.
- 589 35. Teijaro JR, Turner D, Pham Q, Wherry EJ, Lefrancois L, Farber DL. Cutting edge: Tissue-retentive lung
590 memory CD4 T cells mediate optimal protection to respiratory virus infection. *J Immunol.* 2011;187(11):5510-
591 4.
- 592 36. Watano K, Iwabuchi K, Fujii S, Ishimori N, Mitsunashi S, Ato M, et al. Allograft inflammatory factor-1
593 augments production of interleukin-6, -10 and -12 by a mouse macrophage line. *Immunology.*
594 2001;104(3):307-16.
- 595 37. Park JM, Greten FR, Wong A, Westrick RJ, Arthur JS, Otsu K, et al. Signaling pathways and genes that
596 inhibit pathogen-induced macrophage apoptosis--CREB and NF-kappaB as key regulators. *Immunity.*
597 2005;23(3):319-29.
- 598 38. Tang X, Marciano DL, Leeman SE, Amar S. LPS induces the interaction of a transcription factor, LPS-
599 induced TNF-alpha factor, and STAT6(B) with effects on multiple cytokines. *Proc Natl Acad Sci U S A.*
600 2005;102(14):5132-7.
- 601 39. Borovikova LV, Ivanova S, Zhang M, Yang H, Botchkina GI, Watkins LR, et al. Vagus nerve stimulation
602 attenuates the systemic inflammatory response to endotoxin. *Nature.* 2000;405(6785):458-62.
- 603 40. Wang H, Liao H, Ochani M, Justiniani M, Lin X, Yang L, et al. Cholinergic agonists inhibit HMGB1 release
604 and improve survival in experimental sepsis. *Nat Med.* 2004;10(11):1216-21.
- 605 41. van der Zanden EP, Snoek SA, Heinsbroek SE, Stanisor OI, Verseijden C, Boeckxstaens GE, et al. Vagus
606 nerve activity augments intestinal macrophage phagocytosis via nicotinic acetylcholine receptor alpha4beta2.
607 *Gastroenterology.* 2009;137(3):1029-39.e10394.

- 608 42. Su X, Matthay MA, Malik AB. Requisite role of the cholinergic alpha7 nicotinic acetylcholine receptor
609 pathway in suppressing Gram-negative sepsis-induced acute lung inflammatory injury. *J Immunol.*
610 2010;184(1):401-10.
- 611 43. Yang X, Zhao C, Gao Z, Su X. A novel regulator of lung inflammation and immunity: pulmonary
612 parasympathetic inflammatory reflex. *QJM.* 2014;107(10):789-92.
- 613 44. Jiang W, Li D, Han R, Zhang C, Jin WN, Wood K, et al. Acetylcholine-producing NK cells attenuate CNS
614 inflammation via modulation of infiltrating monocytes/macrophages. *Proc Natl Acad Sci U S A.*
615 2017;114(30):E6202-e11.
- 616 45. Turner DL, Bickham KL, Thome JJ, Kim CY, D'Ovidio F, Wherry EJ, et al. Lung niches for the generation
617 and maintenance of tissue-resident memory T cells. *Mucosal Immunol.* 2014;7(3):501-10.
- 618 46. Sastry BV, Sadavongvivad C. Cholinergic systems in non-nervous tissues. *Pharmacol Rev.* 1978;30(1):65-
619 132.
- 620 47. Rosas-Ballina M, Ochani M, Parrish WR, Ochani K, Harris YT, Huston JM, et al. Splenic nerve is required
621 for cholinergic antiinflammatory pathway control of TNF in endotoxemia. *Proc Natl Acad Sci U S A.*
622 2008;105(31):11008-13.
- 623 48. Klapproth H, Reinheimer T, Metzen J, Münch M, Bittinger F, Kirkpatrick CJ, et al. Non-neuronal
624 acetylcholine, a signalling molecule synthesized by surface cells of rat and man. *Naunyn Schmiedebergs Arch*
625 *Pharmacol.* 1997;355(4):515-23.
- 626 49. Pinheiro NM, Miranda CJ, Perini A, Câmara NO, Costa SK, Alonso-Vale MI, et al. Pulmonary
627 inflammation is regulated by the levels of the vesicular acetylcholine transporter. *PLoS One.*
628 2015;10(3):e0120441.
- 629 50. Su X, Lee JW, Matthay ZA, Mednick G, Uchida T, Fang X, et al. Activation of the alpha7 nAChR reduces
630 acid-induced acute lung injury in mice and rats. *American journal of respiratory cell and molecular biology.*
631 2007;37(2):186-92.
- 632 51. Tracey KJ. Physiology and immunology of the cholinergic antiinflammatory pathway. *J Clin Invest.*
633 2007;117(2):289-96.
- 634 52. Sun P, Li L, Zhao C, Pan M, Qian Z, Su X. Deficiency of $\alpha 7$ Nicotinic Acetylcholine Receptor Attenuates
635 Bleomycin-Induced Lung Fibrosis in Mice. *Molecular Medicine.* 2017;23:34-49.
- 636 53. Donovan KM, Leidinger MR, McQuillen LP, Goeken JA, Hogan CM, Harwani SC, et al. Allograft
637 Inflammatory Factor 1 as an Immunohistochemical Marker for Macrophages in Multiple Tissues and
638 Laboratory Animal Species. *Comp Med.* 2018;68(5):341-8.
- 639 54. Frevert CW, Huang S, Danaee H, Paulauskis JD, Kobzik L. Functional characterization of the rat
640 chemokine KC and its importance in neutrophil recruitment in a rat model of pulmonary inflammation. *J*
641 *Immunol.* 1995;154(1):335-44.
- 642 55. Toapanta FR, Ross TM. Impaired immune responses in the lungs of aged mice following influenza
643 infection. *Respir Res.* 2009;10:112.
- 644 56. Wonnacott S. The paradox of nicotinic acetylcholine receptor upregulation by nicotine. *Trends*
645 *Pharmacol Sci.* 1990;11(6):216-9.
- 646 57. Melroy-Greif WE SJ, Ehringer MA. Nicotinic acetylcholine receptors: upregulation, age-related effects,
647 and associations with drug use. *Genes Brain Behav.* 2015.
- 648 58. Hallquist N, Hakki A, Wecker L, Friedman H, Pross S. Differential effects of nicotine and aging on
649 splenocyte proliferation and the production of Th1- versus Th2-type cytokines. *Proc Soc Exp Biol Med.*
650 2000;224(3):141-6.
- 651 59. Cardinali DP, Brusco LI, Selgas L, Esquifino AI. Diurnal rhythms in ornithine decarboxylase activity and
652 norepinephrine and acetylcholine synthesis in submaxillary lymph nodes and spleen of young and aged rats
653 during Freund's adjuvant-induced arthritis. *Brain Res.* 1998;789(2):283-92.
- 654 60. Cardinali DP, Brusco LI, García Bonacho M, Esquifino AI. Effect of melatonin on 24-hour rhythms of
655 ornithine decarboxylase activity and norepinephrine and acetylcholine synthesis in submaxillary lymph nodes
656 and spleen of young and aged rats. *Neuroendocrinology.* 1998;67(5):349-62.

- 657 61. Franceschi C. Inflammaging as a major characteristic of old people: can it be prevented or cured? *Nutr*
658 *Rev.* 2007;65(12 Pt 2):S173-6.
- 659 62. van Beek AA, Van den Bossche J, Mastroberardino PG, de Winther MPJ, Leenen PJM. Metabolic
660 Alterations in Aging Macrophages: Ingredients for Inflammaging? *Trends Immunol.* 2019;40(2):113-27.
- 661 63. Reale M, Iarlori C, Gambi F, Feliciani C, Salone A, Toma L, et al. Treatment with an acetylcholinesterase
662 inhibitor in Alzheimer patients modulates the expression and production of the pro-inflammatory and anti-
663 inflammatory cytokines. *Journal of Neuroimmunology.* 2004;148(1):162-71.
- 664 64. Reale M, Iarlori C, Gambi F, Lucci I, Salvatore M, Gambi D. Acetylcholinesterase inhibitors effects on
665 oncostatin-M, interleukin-1 β and interleukin-6 release from lymphocytes of Alzheimer's disease patients.
666 *Experimental Gerontology.* 2005;40(3):165-71.
- 667 65. Kokras N, Stamouli E, Sotiropoulos I, Katirtzoglou EA, Siarkos KT, Dalagiorgou G, et al. Acetyl
668 Cholinesterase Inhibitors and Cell-Derived Peripheral Inflammatory Cytokines in Early Stages of Alzheimer's
669 Disease. *J Clin Psychopharmacol.* 2018;38(2):138-43.
- 670 66. Bhattacharjee S, Patanwala AE, Lo-Ciganic W-H, Malone DC, Lee JK, Knapp SM, et al. Alzheimer's
671 disease medication and risk of all-cause mortality and all-cause hospitalization: A retrospective cohort study.
672 *Alzheimers Dement (N Y).* 2019;5:294-302.
- 673 67. Abe Y, Shimokado K, Fushimi K. Donepezil is associated with decreased in-hospital mortality as a result
674 of pneumonia among older patients with dementia: A retrospective cohort study. *Geriatrics & Gerontology*
675 *International.* 2018;18(2):269-75.



bioRxiv preprint doi: <https://doi.org/10.1101/2020.07.02.184226>; this version posted July 2, 2020. The copyright holder for this preprint (which was not certified by peer review) is the author/funder, who has granted bioRxiv a license to display the preprint in perpetuity. It is made available under aCC-BY 4.0 International license.

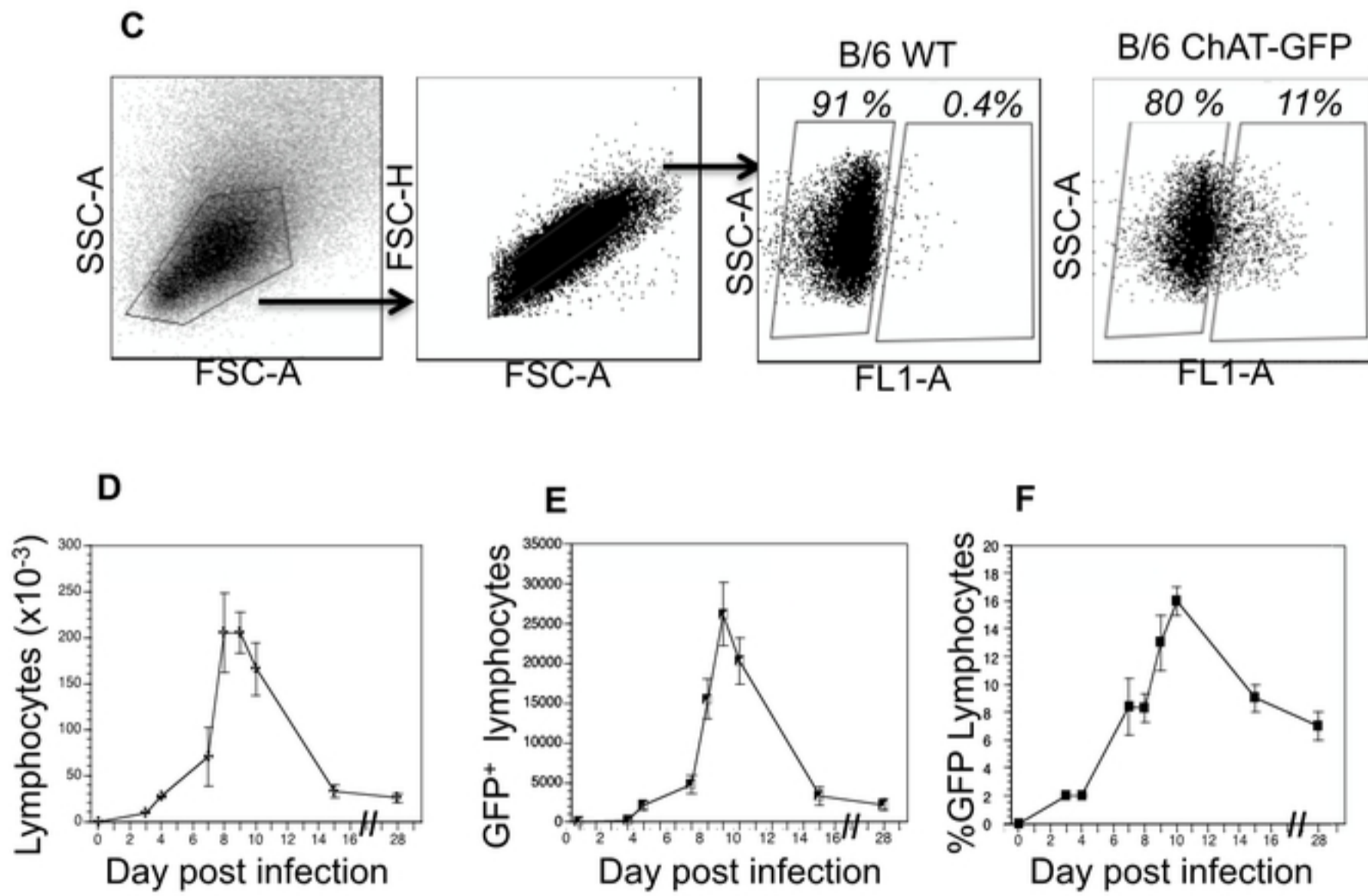


Fig 1

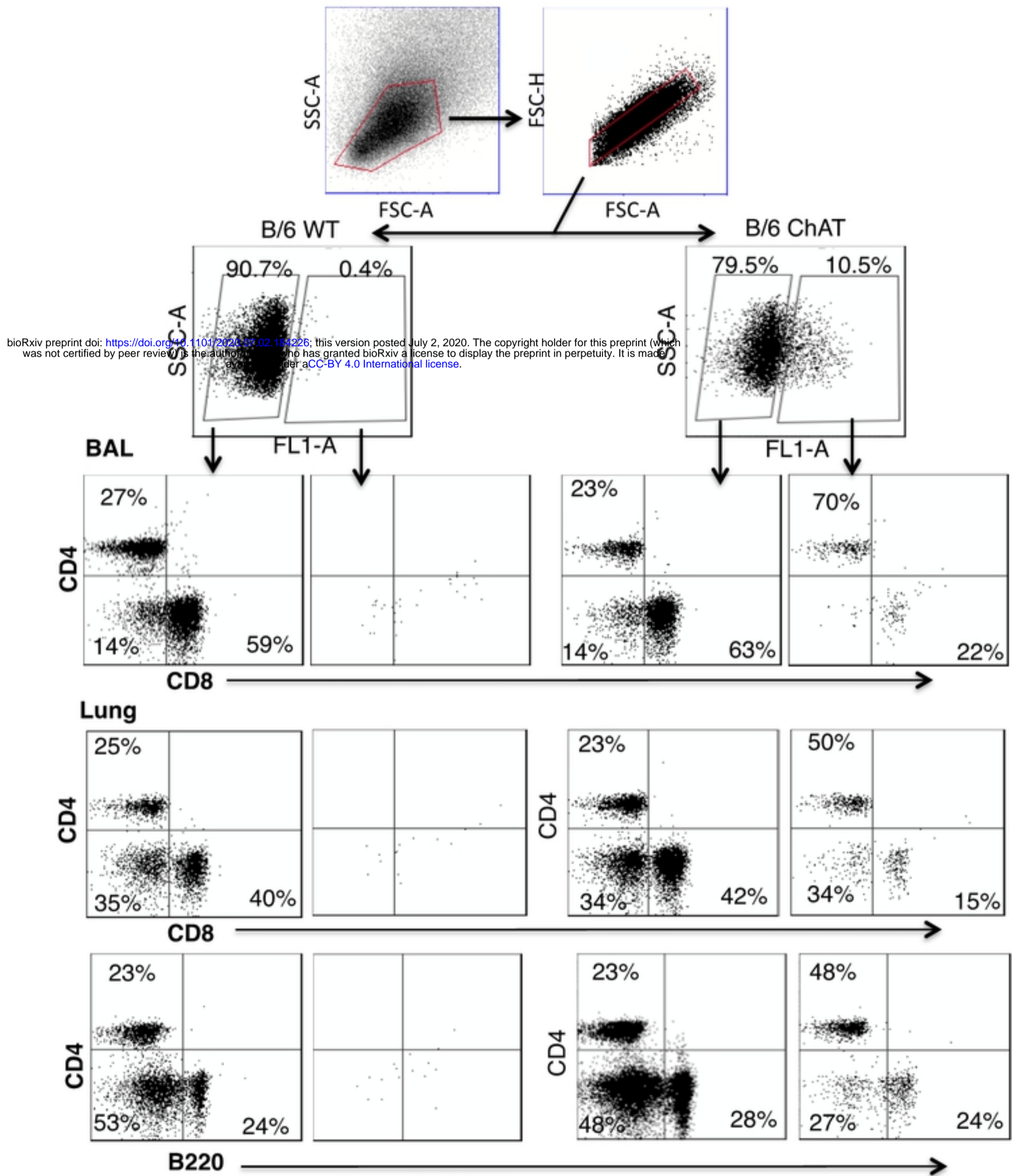


Fig 2

bioRxiv preprint doi: <https://doi.org/10.1101/2020.07.02.184226>; this version posted July 2, 2020. The copyright holder for this preprint (which was not certified by peer review) is the author/funder, who has granted bioRxiv a license to display the preprint in perpetuity. It is made available under aCC-BY 4.0 International license.

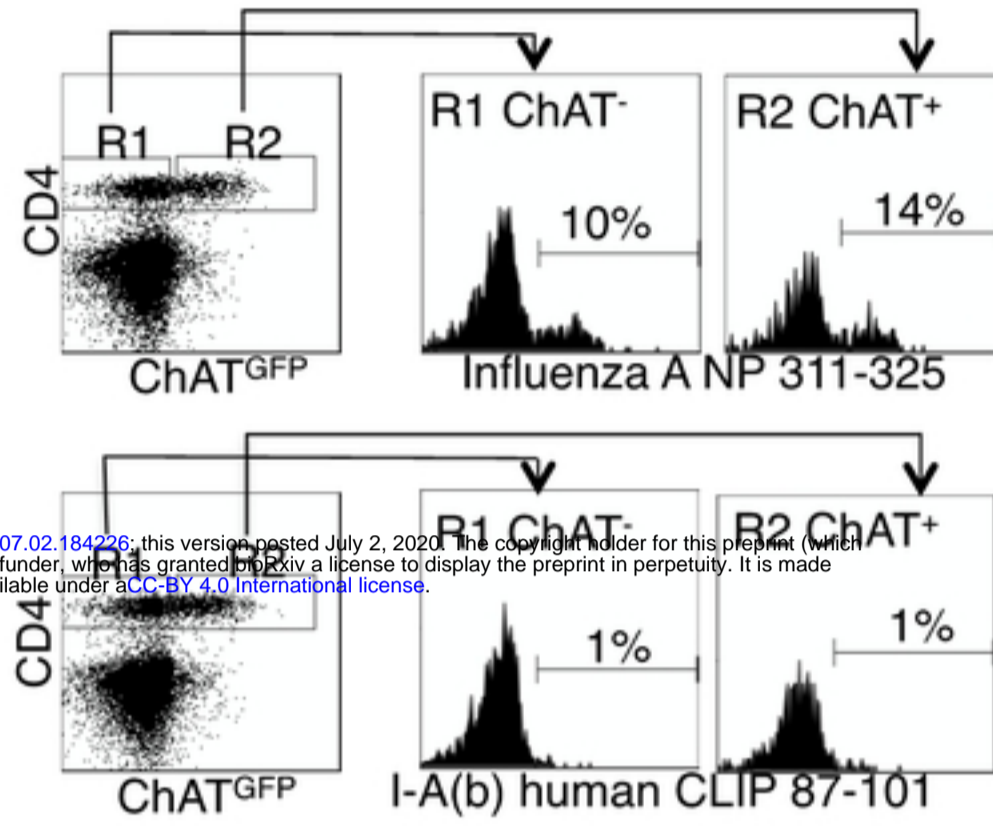
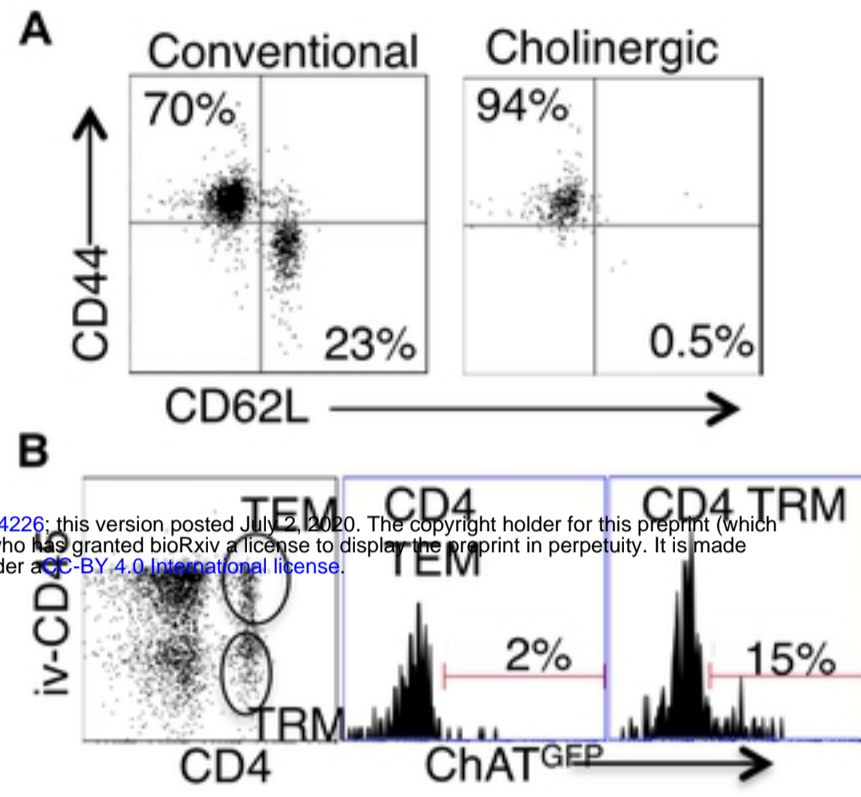


Fig 3

bioRxiv preprint doi: <https://doi.org/10.1101/2020.07.02.184226>; this version posted July 2, 2020. The copyright holder for this preprint (which was not certified by peer review) is the author/funder, who has granted bioRxiv a license to display the preprint in perpetuity. It is made available under aCC-BY 4.0 International license.



bioRxiv preprint doi: <https://doi.org/10.1101/2020.07.02.184226>; this version posted July 2, 2020. The copyright holder for this preprint (which was not certified by peer review) is the author/funder, who has granted bioRxiv a license to display the preprint in perpetuity. It is made available under aCC-BY 4.0 International license.

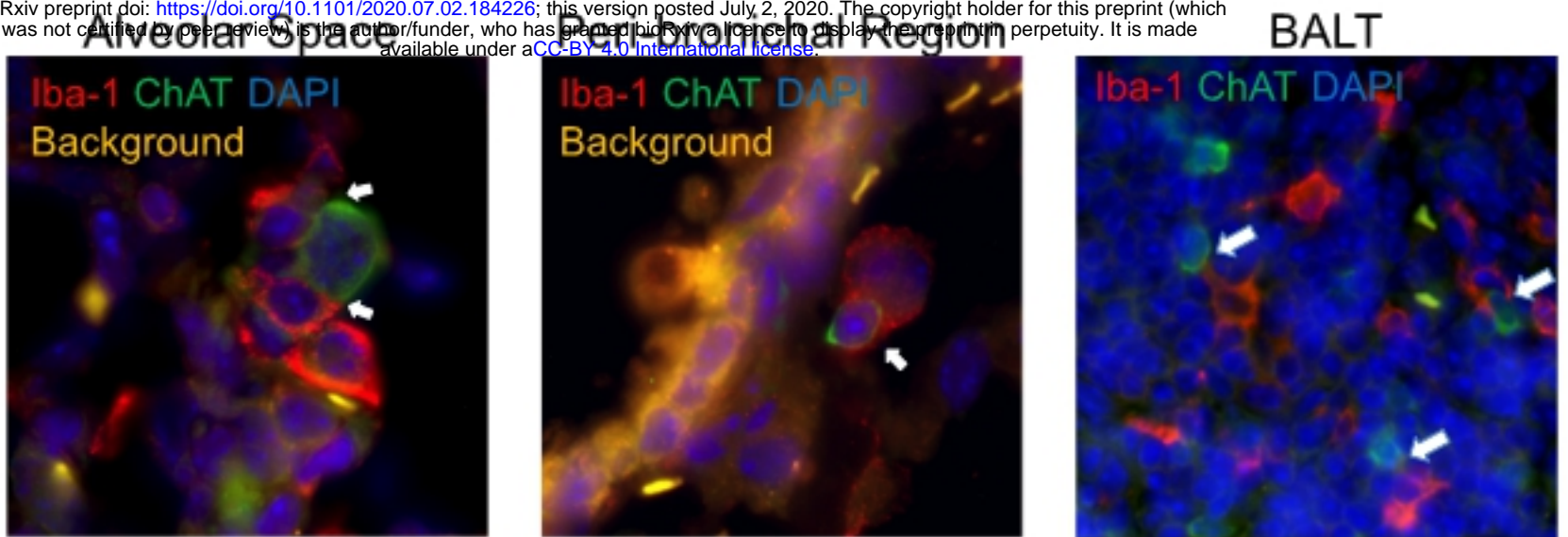


Fig 5

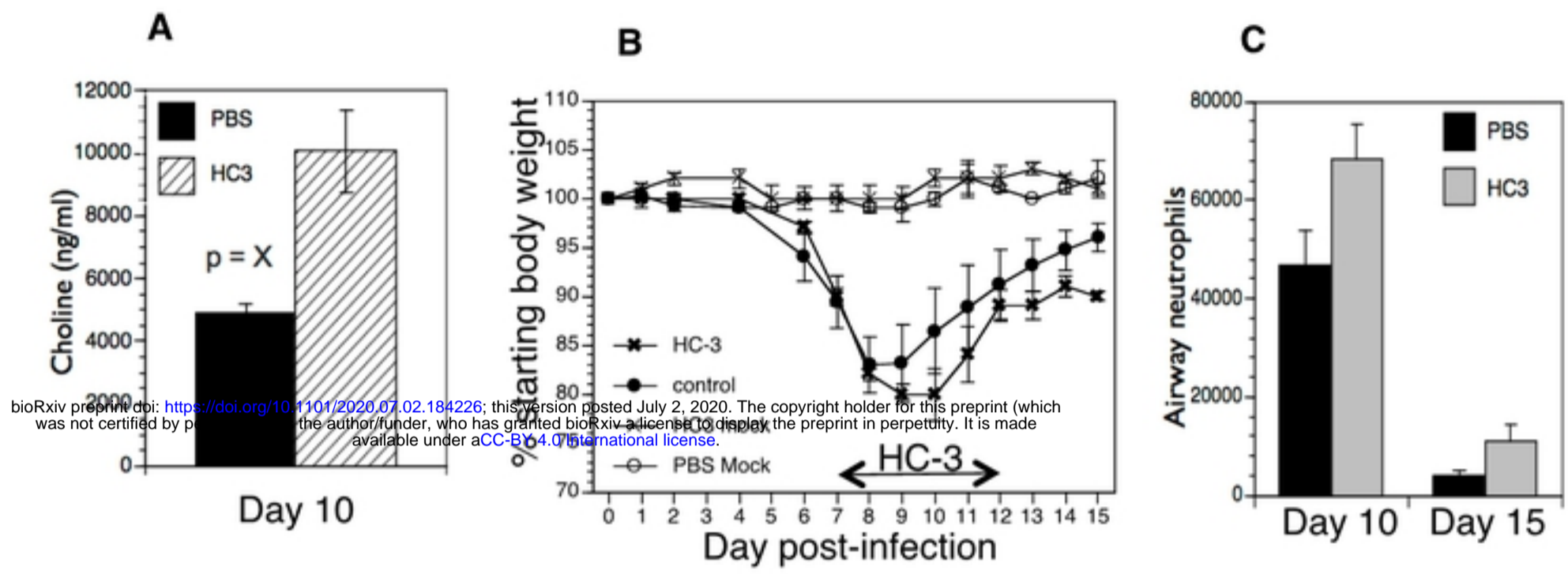


Fig 6

bioRxiv preprint doi: <https://doi.org/10.1101/2020.07.02.184926>; this version posted July 2, 2020. The copyright holder for this preprint (which was not certified by peer review) is the author/funder, who has granted bioRxiv a license to display the preprint in perpetuity. It is made available under aCC-BY 4.0 International license.

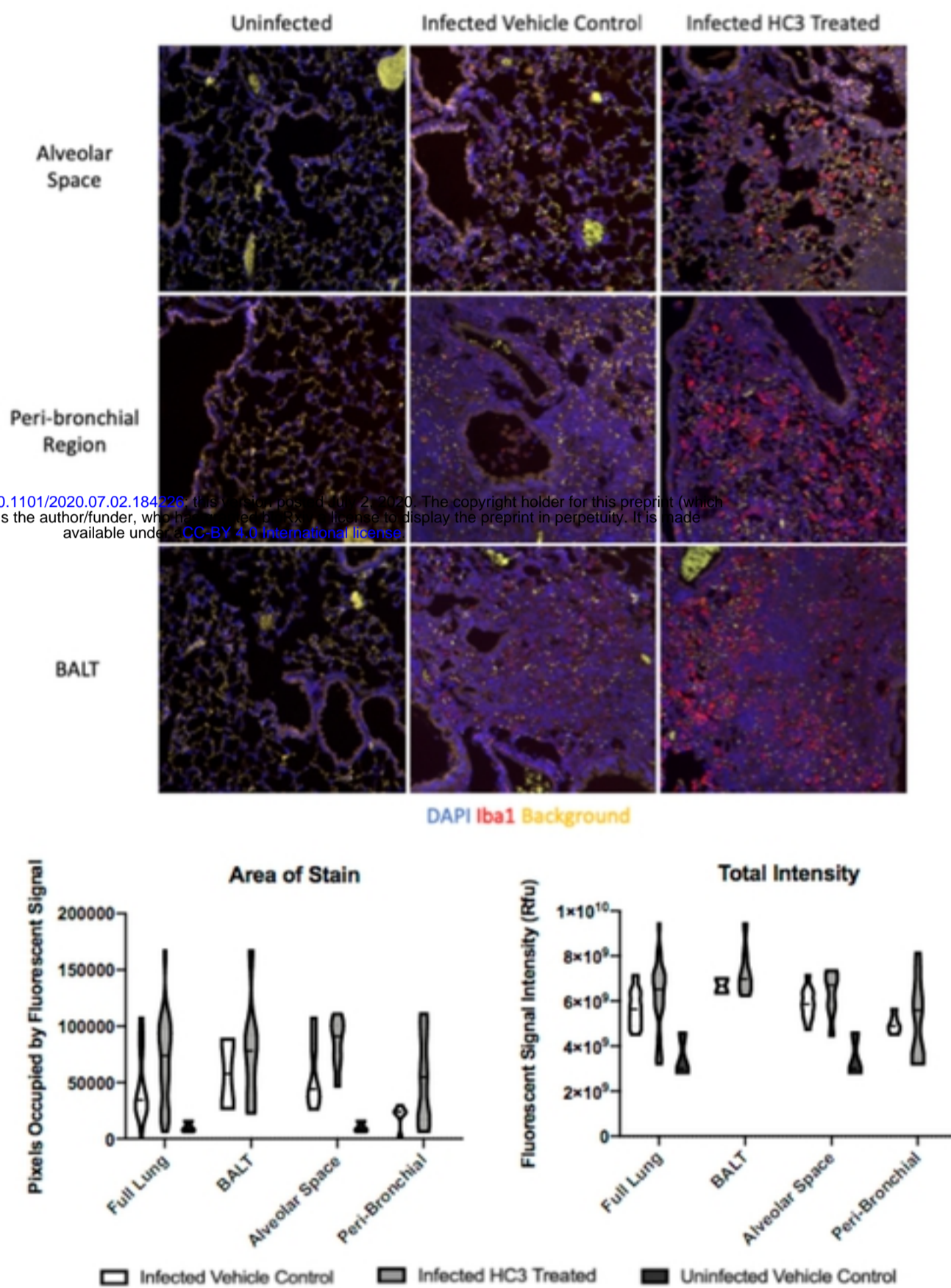


Fig 7

bioRxiv preprint doi: <https://doi.org/10.1101/2020.07.02.184226>; this version posted July 2, 2020. The copyright holder for this preprint (which was not certified by peer review) is the author/funder, who has granted bioRxiv a license to display the preprint in perpetuity. It is made available under aCC-BY 4.0 International license.

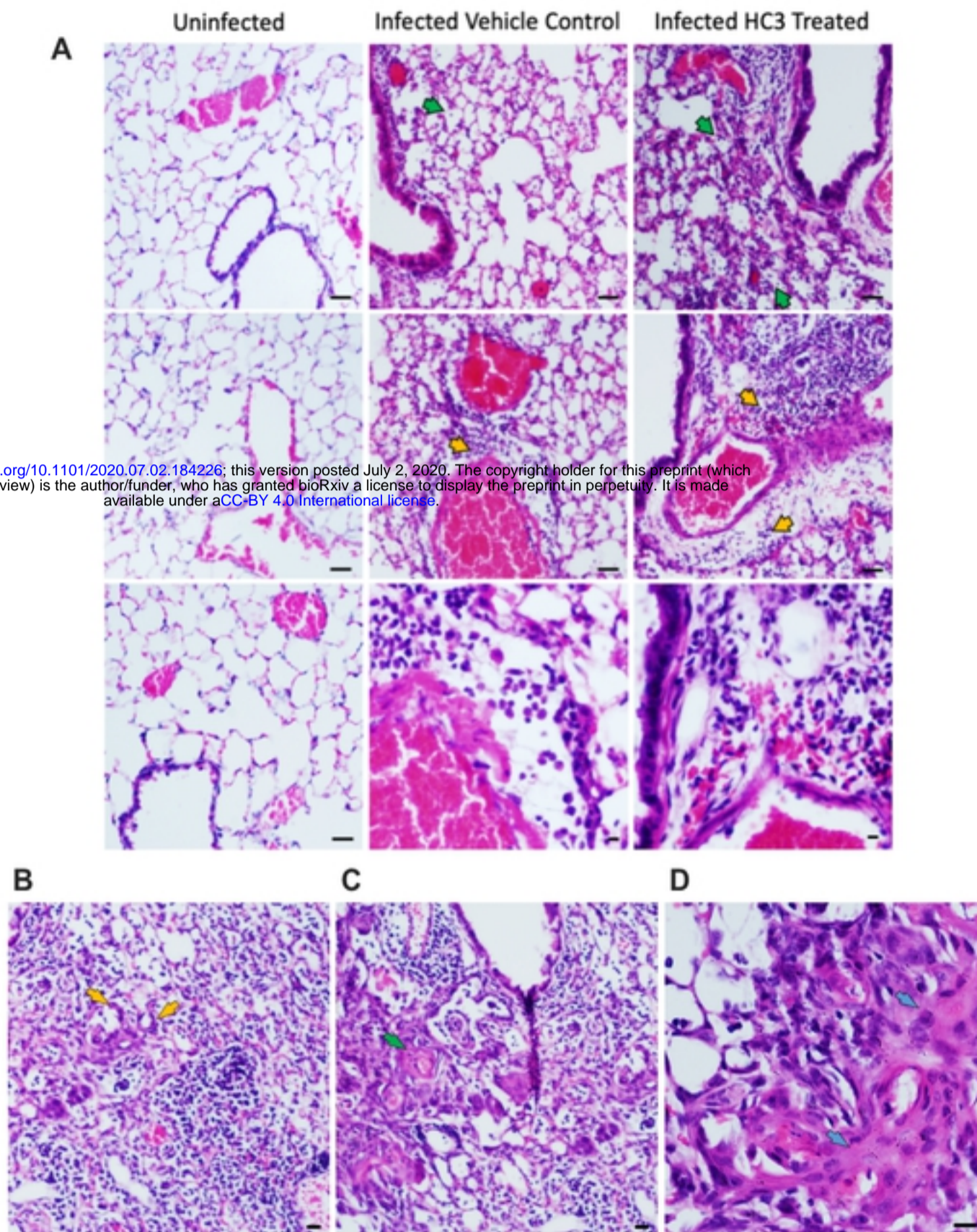


Fig 8